Investigation and modeling of tensile failure properties of wound ceramic matrix composites

Yuan Shi*, Neraj Jain, Dietmar Koch

Institute of Structures and Design, German Aerospace Center, Stuttgart, Germany

A B S T R A C T

The paper presents enhanced studies of investigation and modeling of failure properties for wound ceramic matrix composites with varied fiber orientations under tensile loading. Based on mechanical tests and microstructure analysis, the characteristics of a virtual equivalent unidirectional layer (UD-layer) were examined and treated as input for modified Tsai-Wu failure criterion. In order to predict the mechanical properties with more accuracy, particular features of the investigated material have to be taken into consideration: definition of two material modeling groups based on the analysis of microstructure; interaction between failure strength and strain through inelastic deformation; inclusion of inhomogeneities created due to the manufacturing process in the analytical model. Based on the good correlation between the experiments and the modeling results, it can be shown that modeling approaches, considering the above mentioned particular material features, allow a very accurate prediction of the mechanical properties under in-plane tensile loading of CMC laminates.

1. Introduction and objective

Ceramic Matrix Composites (CMCs) have gained attention of material development researchers in recent years, because of their favorable mechanical properties at high temperature and comparatively low density. By using the excellent high temperature properties of ceramic fiber and ceramic matrix, CMC materials exceed all other materials in that field of interest [1–4]. Due to its high flexibility (winding angle from 0° to 90°), net shape fabrication and relatively low cost, the winding technique has been successfully implemented for the production of complex CMC components with stress-oriented fiber alignment and rotational symmetry axis in different areas [5–9].

Due to the complex anisotropic in-plane mechanical behavior, the accurate prediction and assessment of the material properties of CMC components, such as the material WHIPOX™ (Wound HIghly Porous OXide Ceramic) investigated in this work, has to be supplemented by advanced modeling approaches. Being based on the material homogenization techniques, meso- and microscopic methods by using Representative Volume Unit (RVU), Classical Laminate Theory (CLT) and classic failure criterion allow a good estimation of elastic properties [10–13], maximal loading capacity [14,15] and progressive damage [16,17] in composite material. Furthermore, characterization and modeling of fatigue behavior of different composites with consideration of different fiber orientation and frequency have been investigated in [18–22]. In comparison with the fiber reinforced polymeric composites, the main problem of modeling of failure properties for wound CMCs is the lack of data concerning individual unidirectional layers (UD-layer). The production and characterization of characteristic CMC UD-materials is almost impossible because of the non-typical unhindered shrinkage of matrix, transverse to the fibers, during the production process. This prevents the UD-material from being considered as a representative material for modeling approaches for CMCs.

Due to the above mentioned problem, advanced modeling approaches with virtual equivalent UD-layer properties have to be created for the evaluation and prediction of the material behavior of wound CMC components. The previous studies of Shi et al. [23,24] have shown that the elastic properties of the equivalent UD-layer can be evaluated through the inverse approach of CLT, which are suitable for the determination and prediction of the elastic properties of wound CMCs with different microstructures and various fiber orientations. In comparison, the present work focuses on the investigation and modeling of tensile failure properties for wound CMCs through modified Tsai-Wu failure criterion.

Based on the relationship between models and the physical behavior of composites, failure criterion can be classified as either physically based or non-physically based models. Several physically based criteria have been developed in the last years. One of the most important is the work of Puck in [15]. According to his hypothesis, two basically

* Corresponding author.
E-mail address: yuan.shi@dlr.de (Y. Shi).

independent criteria are applied: one for fiber failure (FF) and the second for inter-fiber failure (IFF). The latter one includes the matrix cracks and interface failure between fiber and matrix. Furthermore, based on the stress invariants, the behavior of five different failure modes can be calculated by Cuntze model with consideration of probability of failure [25]. Generally, to evaluate the inclination of the fracture surface at zero normal stress using the Puck failure criterion or Cuntze model, strength values and additional material parameters are required. Due to the lack of recommendations for these inclination parameters (e.g. in [26]) for CMCs, it is particularly difficult to apply the physically based failure criterion for the investigated WHIPOX™ material or other CMCs. Furthermore, due to the fact that the Puck failure criterion was developed on the basic structure element of fiber reinforced polymeric composites, the UD-layer, identification of the failure mechanism through Puck method may not be suitable for CMCs with braided, wound or woven structure. On the other hand, the non-physically based models have been developed and discussed during the past century. The most commonly applied hypothesis is the Tsai-Wu failure criteria [14], which proposes quadratic fracture conditions with interpolation functions for laminates by considering interactions between different components of the stress and strain tensors. Based on this idea, a polynomial tensor can be used to describe the failure surface. Considerable effort has been put into the development of suitable models to reliably predict the failure of fiber reinforced composites (e.g. compiled in [27–29] and reviewed in [30]). It should be noticed that the attempt to develop a universal failure criterion for all fiber composites with any desired laminate structures has resulted in a confusingly large number of failure criteria for composite design engineers. No recommendation for a choice can be given because none of the criteria is substantiated by sufficient experimental evidence. Furthermore, the commonly discussed failure criteria were designed for fiber reinforced polymer matrix composites and not for CMCs.

The production and characterization of the representative UD-layer is a challenge for CMC materials. Therefore, instead of a real UD-layer, a virtual equivalent UD-layer was implemented in the Tsai-Wu quadratic failure criterion. In this work, based on the mechanical characterization and analysis of microstructure, modified Tsai-Wu method for the modeling of the tensile failure properties has been developed. The efficiency of the model has been demonstrated by the investigated material WHIPOX™ with different winding angle.

2. Material and experiment

2.1. Material WHIPOX™

The investigated material WHIPOX™ is a continuous fiber reinforced oxide/oxide ceramic composite, which represents one variant of an oxide fiber reinforced ceramic matrix composite. It was developed and produced by Institute of Materials Research, German Aerospace Center, Cologne. WHIPOX™ components are manufactured by a computer controlled filament winding process with slurry infiltration of ceramic fiber bundles. The winding process allows a variable shape with regards to the core, thereby forming the component and the architecture of the fiber reinforcement. Fig. 1a shows an initial stage of WHIPOX™ winding with angles of ± 45°. A key advantage of wound CMCs is its in-plane anisotropic material behavior, which strongly depends on the winding angle $\pm\theta^{\circ}$, defined between the longitudinal axis X of the wound preforms and the fiber tows direction (see Fig. 1b).

The manufacturing process for even plates is carried out in five steps: matrix infiltration of fiber tows, winding with angles defined to the cylindrical preform (green body), cutting and flat lay-up, drying and then sintering for about 1 h at 1300 °C [8,31]. Although the green body is quite flexible in the wet state, the flattening and the forming of the laminate may lead to rearrangement of the filament bundles and therefore resulting in microstructural inhomogeneity. A WHIPOX™ plate with a schematic representation of the winding structure and winding angle $\pm\theta^{\circ}$ has been shown in Fig. 1b. Table 1 lists the material composition of WHIPOX™. The fiber volume content (FVC) and the porosity (e') fluctuate in a wide range. The individual values of the respective WHIPOX™ plates have been summarized in Table 3. A typical microstructure of WHIPOX™ is shown in Fig. 2. The highly porous matrix of WHIPOX™ is aimed to a possible notch insensitive and damage tolerant behavior.

Due to the microstructure of WHIPOX™, the calculation and modeling of material behavior encounter two challenges. The majority of WHIPOX™ structure has a layer-like design; however, the winding processing induces crossing lines where the fiber bundle intersections are to be found in WHIPOX™ structure (see Fig. 1b). The relationship between the structure of these areas and the mechanical properties of WHIPOX™ is presented in [32]. In this work, an equivalent UD-layer with the mixed characteristics of layer-like design and crossing lines has been presented and used for the modeling of tensile failure properties of WHIPOX™. Another challenge of WHIPOX™ microstructure for modeling is that the experimentally determined transverse stiffness (perpendicular to the fiber direction) of the “quasi” UD-material (e.g. ± 3°) does not reflect the circumstance in a layer structure with alternating fiber orientations [33]. This is especially true for fiber architectures with increasingly vertical sloping of the two fiber directions, particularly 0°/90° (winding angle ± 45°). The reason for this difference is the shrinkage cracks in the WHIPOX™ matrix, which have been thoroughly discussed in the previous study [23,24]: during the sintering process of WHIPOX™, shrinkage of the matrix is blocked by the stiff fibers of adjacent layers; The maximum hindering of shrinkage is reached at high winding angles, e.g. ± 45° (0°/90°) winding. This leads to cracking of the matrix during sintering and thus the reduction of material properties in the transverse direction. Micro Computed Tomography (μCT) was applied for the analysis of shrinkage cracks for different winding angles. Based on the previous results of microstructure analysis of matrix cracks [23,24], no monotonic increase of the crack density in relation to winding angle can be observed. A transition line between the matrix with and without cracks can be found in the winding angle of ± 30°. No cracks were observed for smaller winding angles. WHIPOX™ with winding angles of ± 30° through ± 45 showed similar crack distributions. Therefore, the modeling of the mechanical properties of WHIPOX™ was divided into two classes: WHIPOX™ with matrix cracks (WC) and WHIPOX™ without matrix cracks (NC).

2.2. Tensile test

The essential material properties under tensile load were determined and evaluated using mechanical in-plane tensile testing. The samples for the experiments were cut from flat plates with varied fiber orientations. All the tests were performed at room temperature in air under quasi-static loading. Table 2 gives an overview of the performed tensile test and the investigated orientations relative to the specimen's longitudinal axis. The specimens with the dimensions of $150 * 10(8) * 5\,mm^3$ in Table 2 were produced with a reduced cross section in their gauge areas in order to prevent failure in the clamping section and to assure failure in their center regions. For the tensile test, the longitudinal and transverse strains were measured with strain gauges. The experimental tests for the investigated orientation ± 3°/ ± 87° in this study were conducted at Institute of Materials Research, German Aerospace Center Cologne. The other experiments were performed up to failure of sample on a universal testing machine (Zwick 1494) at a controlled cross head speed of 1 mm/min. The failure stress was calculated from the maximum load.

3. Modeling approach

3.1. Tsai-Wu failure criterion in stress space

The failure envelope in the stress space of the Tsai-Wu failure

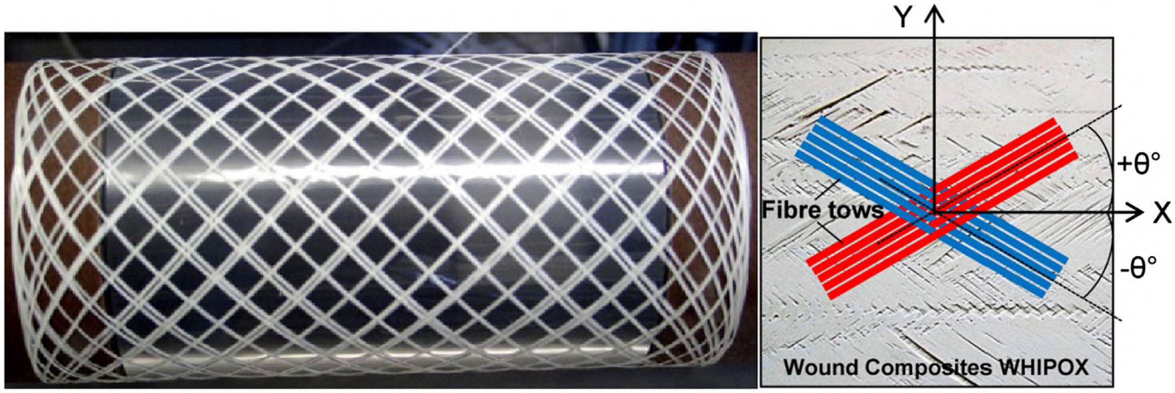

a) b)

Fig. 1. Initial stage of winding process for WHIPOX™ material [48] and (b) WHIPOX™ plate with schematic representation of winding structure and winding angle ± θ° [24]. (For interpretation of the references to colour in this figure legend, the reader is referred to the web version of this article.)

Table 1
Material composition of WHIPOX™.

Fiber type	Nextel™ 610 (Al_2O_3)
Fiber diameter	Approx. 12 µm
Fiber bundles	3000 DEN
Fiber volume content	34.0–43.0%
Matrix	Al_2O_3
Open porosity of composite	18.0–32.0%

criterion can be described as [14]:

$$F_i\sigma_i + F_{ij}\sigma_i\sigma_j = 1 \tag{1}$$

where $i, j = 1, 2, \cdots, 6$; F_i and F_{ij} are strength tensors of the second and fourth rank, respectively.

For an orthotropic ply subjected to conditions of plane stress, the general Tsai-Wu quadratic criterion in stress space can be written as:

$$F_1\sigma_1 + F_2\sigma_2 + F_{11}\sigma_1^2 + F_{22}\sigma_2^2 + F_{66}\tau_{12}^2 + 2F_{12}\sigma_1\sigma_2 = 1 \tag{2}$$

The strength parameters F_1 to F_{66} from Eqs. (1) and (2) are related to the engineering strengths of the UD-layer [14], is this work, the equivalent UD-layer in Fig. 3: F_1 and F_{11} can be determined through the ultimate strength of the UD-layer in 1-axis (local coordinate system in Fig. 3) with σ_1^T tensile strength and σ_1^C compressive strength. Similar in 2-axis: F_2 and F_{22} can be determined through the strengths σ_2^T under tensile and σ_2^C under compressive stress. F_{66} is connected with shear strength τ_{12}.

Generally a failure envelope must be closed in order to avoid infinite strength values. In the case of Tsai-Wu strength criterion, an interaction term F_{12} is bound to ensure that the failure envelope is closed. The value of F_{12} has to be determined through bi-axial tensile test. When equal tensile loads and no shear loads are applied along the two principal material axes in a unidirectional lamina, F_{12} is obtained via:

$$F_{12} = \frac{1}{2}\left[\frac{1}{(\sigma_{bi})^2} - \frac{F_1 + F_2}{\sigma_{bi}} - (F_{11} + F_{22})\right] \tag{3}$$

where σ_{bi} is the failure load during the bi-axial tensile test. Because of the difficulty in performing combined stress tests, some empirical estimations of the F_{12} value have been proposed for different failure criteria and summarized in [34] and the effect of F_{12} on the Tsai-Wu failure envelopes has been studied elsewhere [35–37]. In a paper on Tsai-Wu failure criterion [38], F_{12} may be considered as zero if it falls in the range $\pm 6 \cdot 10^{-5}$, based on the test results of unidirectional graphite/epoxy samples. According to the studies of Narayanaswami and Adelman [39], the interaction parameter of composite material is small and can be often taken as zero. This conclusion drawn from the negligible interaction parameter has been generally accepted as being applicable to different composite materials [40,41]. In the case of investigated WHIPOX™ material, the interaction term F_{12} has been set to zero due to the lack of possibility to produce actual unidirectional layer and perform bi-axial tensile testing. Eq. (2) can be reduced to:

$$F_1\sigma_1 + F_2\sigma_2 + F_{11}\sigma_1^2 + F_{22}\sigma_2^2 + F_{66}\tau_{12}^2 = 1 \tag{4}$$

The original form of Tsai-Wu failure criterion with Eq. (1) could only predict the final failure of the material. In order to analyze the progressive failure mode, a strength ratio R has been defined in [35]. The ratio R is a linear scaling factor and related to the loading applied from any state of stress:

Table 2
Tensile specimen geometry with dimensions, loading direction and the investigated orientations.

Test	Test geometries, dimensions and loading direction	Investigated orientations θ
Tensile	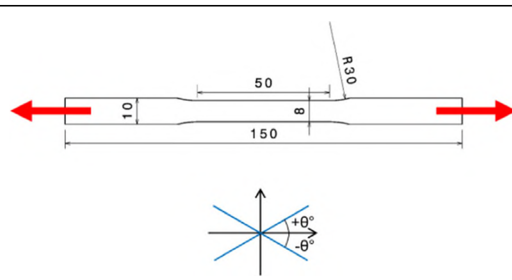	± 3°[a] ± 15°/ ± 75°, ± 22.5°/ ± 67.5°, ± 30°/ ± 60° and ± 45°

[a] The experimental tests for the investigated orientation ± 3° in this study were conducted in Institute of Materials Research, German Aerospace Center Cologne.

Table 3
Fiber volume content (*FVC*) and open porosity (e') of different plates, strength and fracture strain values in directions $\boldsymbol{x}$ and $\boldsymbol{y}$ obtained from tensile tests with different winding angles.

Plate	Test direction	*FVC* [%]	e' [%]	σ_x [MPa]	σ_y [MPa]	ε_x [%]	ε_y [%]
WF3	± 3°	42.7	22.0	289.0 ± 14.7	–	0.14 ± 0.01	–
BT15	± 15° (± 75°)	41.2	27.9	276.8 ± 4.9	22.1 ± 3.8	0.14 ± 0.01	0.02 ± 0.01
BT225	± 22.5° (± 67.5°)	39.1	18.5	233.4 ± 35.7	37.0 ± 3.6	0.12 ± 0.01	0.03 ± 0.01
BT30	± 30° (± 60°)	34.0	31.4	133.5 ± 18.5	27.7 ± 2.8	0.12 ± 0.03	0.07 ± 0.01
BT45	± 45°	40.5	29.1	96.4 ± 8.5	96.4 ± 8.5	0.13 ± 0.02	0.13 ± 0.02

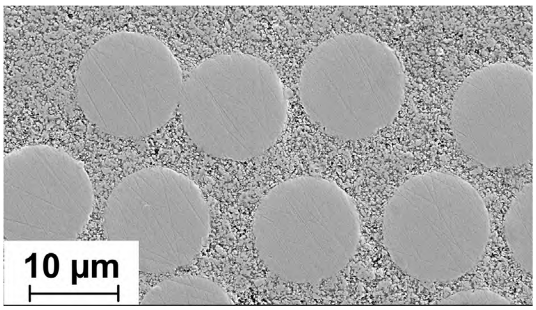

Fig. 2. Microstructure of WHIPOX™ with fiber cross section and highly porous matrix.

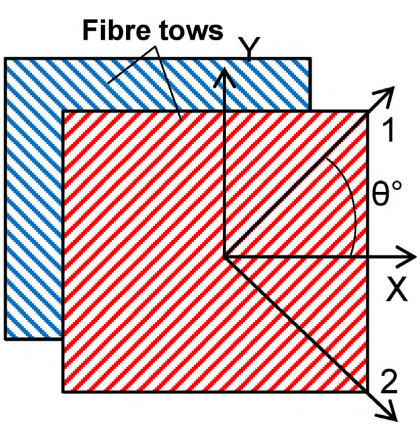

Fig. 3. Equivalent UD-layers with the local coordinate system, 1-axis in fiber direction and 2-axis in perpendicular direction. (For interpretation of the references to colour in this figure legend, the reader is referred to the web version of this article.)

$$R\sigma^{app} = \sigma^{max} \tag{5}$$

where σ^{app} is the current applied stress and σ^{max} is the strength value of the material. Obviously, failure occurs when $R = 1$. By substituting the maximum stress components $\sigma_i = \sigma_i^{max}$ and $\sigma_j = \sigma_j^{max}$ with the relationship between applied stress and strength to the original Tsai-Wu failure Eq. (1), the value of the ratio R can be easily determined with the quadratic equation [35]:

$$(F_{ij}\sigma_i\sigma_j)R^2 + (F_i\sigma_i)R - 1 = 0 \tag{6}$$

In addition, a reciprocal failure index k was defined as being the inverse value of R with $k = 1/R$ [35]. The original Tsai-Wu form can be described as:

$$(F_{ij}\sigma_i\sigma_j)\left(\frac{1}{k}\right)^2 + (F_i\sigma_i)\left(\frac{1}{k}\right) - 1 = 0 \tag{7}$$

3.2. Tsai-Wu failure criterion in strain space

Compared to Tsai-Wu failure criterion in stress space, the criterion in strain space is more convenient because the distribution of strain across the thickness of a laminate is assumed to be constant. Therefore, fracture strain of any ply in a laminate can be easily determined by applying the failure criterion in strain space. In the case of linear elastic behavior up to failure, the one-to-one correspondence between stress and strain is always available. The stress value at each state of load can essentially have only one corresponding strain. For an orthotropic material, Tsai-Wu stress failure criterion in Eq. (1) can be represented in strain components as [42]:

$$F_i\sigma_i + F_{ij}\sigma_i\sigma_j = F_i[Q_{ik}\varepsilon_k] + F_{ij}[Q_{ik}\varepsilon_k][Q_{jl}\varepsilon_l] = [F_iQ_{ik}]\varepsilon_k + [F_{ij}Q_{ik}Q_{jl}]\varepsilon_k\varepsilon_l$$
$$= G_k\varepsilon_k + G_{kl}\varepsilon_k\varepsilon_l = 1 \tag{8}$$

where G_k and G_{kl} are strain tensors of the second and fourth rank, respectively, and can be determined [42]:

$$G_k = F_iQ_{ik} \tag{9}$$

$$G_{kl} = F_{ij}Q_{ik}Q_{jl} \tag{10}$$

The same strength ratio R and failure index k can be determined from the quadratic criterion in strain space [42]:

$$(G_{kl}\varepsilon_k\varepsilon_l)R^2 + (G_k\varepsilon_k)R - 1 = 0 \tag{11}$$

$$(G_{kl}\varepsilon_k\varepsilon_l)\left(\frac{1}{k}\right)^2 + (G_k\varepsilon_l)\left(\frac{1}{k}\right) - 1 = 0 \tag{12}$$

On the other hand, as it is the case of the non-linear elastic behavior up to failure, stress and strain do not correspond directly to initial material stiffness matrix Q_{ij}. Since the stiffness values are usually degraded after a certain load state for non-linear behavior, any calculated strain values using initial material stiffness would be underestimated. In order to model the inelastic strain, an inelastic deformation factor Δ_k is introduced in Section 3.3.

3.3. Inelastic deformation

In the case of non-linear elastic behavior up to failure, stress and strain cannot be directly tied to the initial material stiffness matrix Q_{ij}. The Classic Laminate Theory and the Tsai-Wu failure criterion are restricted to linear elastic behavior of the composite. This does not allow the calculation of failure strain in non-linear elastic behaviors of laminates. Therefore, an empirical modeling approach has been developed to calculate the failure strain of the laminate with non-linear elastic behavior.

The aim of this modeling approach is to predict failure strain under varying orientations for investigated WHIPOX™ material. In order to explain the approach, a typical tensile stress-strain behavior of WHIPOX™ laminate with non-linear elastic behavior is shown in Fig. 4. Since the failure strength σ_{test} can be calculated through Tsai-Wu failure criterion in stress space, the strain value ε_{linear} calculated through the initial material stiffness E is underestimated when compared to the failure strain ε_{test}. This difference is observed in the behavior of the investigated material WHIPOX™ with different fiber orientations and a trend is noticed. An inelastic deformation factor Δ_k is apparently a relationship between the two different strain values ε_{linear} and ε_{test}. This inelastic deformation factor Δ_k for each layer k with different fiber orientation in a particular laminate can be illustrated through the

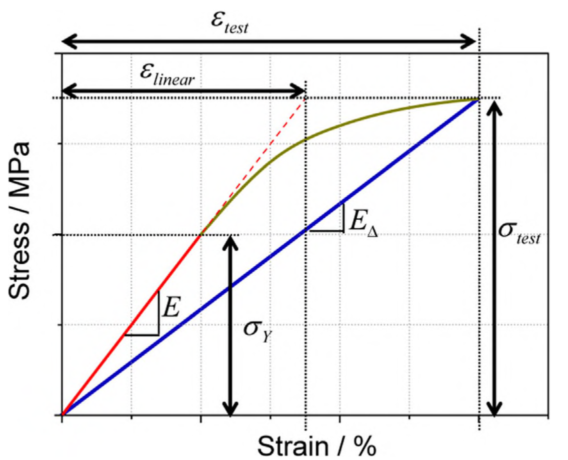

Fig. 4. Tensile stress-strain behavior of a typical WHIPOX™ laminate with non-linear elastic behavior. (For interpretation of the references to colour in this figure legend, the reader is referred to the web version of this article.)

equation:

$$\Delta_k = \frac{\varepsilon_{linear}}{\varepsilon_{test}} \tag{13}$$

Obviously, there is linear elastic behavior up to failure if $\Delta_k = 1$. According to the test results in the following Section 4.1, the value of factor Δ_k is strongly dependent on the fiber orientation. On the other hand, since WHIPOX™ material does not show a distinctive yield point in any direction, the virtual yield stress σ_Y in Fig. 4 was defined as the function of factor Δ_k and failure strength σ_{test}:

$$\sigma_Y = \sigma_{test}\Delta_k \tag{14}$$

According to the classical laminate theory the relationship between strain $\{\varepsilon^0\}$, curvature $\{\kappa\}$, resultant force $[N_{x,y,xy}]$ and moment $[Mo_{x,y,xy}]$ under in-plane loading can be described with the individual in-plane sub-matrices of the stiffness matrix $[\overline{Q}_{ij}]$ for a multilayer laminate [43]. The individual in-plane sub-matrices of $[\overline{Q}_{ij}]$ are: strain stiffness $[S_{ij}]$, coupling stiffness$[C_{ij}]$ and bending stiffness $[B_{ij}]$. They were determined through the stiffness matrix of a single UD-layer with a thickness of t_k [43]:

$$S_{ij} = \sum_{k=1}^{N} (\overline{Q}_{ij})_k t_k \tag{15}$$

$$C_{ij} = \sum_{k=1}^{N} (\overline{Q}_{ij})_k t_k \overline{Z}_k \tag{16}$$

$$B_{ij} = \sum_{k=1}^{N} (\overline{Q}_{ij})_k (t_k \overline{Z}_k^{\,2} + t_k^{\,3}/12) \tag{17}$$

The factor Δ_k is considered to be a property of each layer in a particular laminate. It is effectively a factor which indicates change in stiffness within the material. Since a composite comprises of several layers with varying fiber orientation, e.g. a laminate has two layers with different fiber orientation 15° and 45°, the stiffness is different in each layer k and the corresponding stiffness change has to be introduced while applying the Classical Laminate Theory considering stiffness of each and every layer. Therefore, it is reasonable to use Δ_k when the layer properties are assembled by individual sub-matrices: strain stiffness $[S_{ij}]$, coupling stiffness $[C_{ij}]$ and bending stiffness $[B_{ij}]$. Eqs. (15)–(17) are rewritten as:

$$(S_{ij})_{\Delta_k} = \sum_{k=1}^{N} (\overline{Q}_{ij})_k t_k \Delta_k \tag{18}$$

$$(C_{ij})_{\Delta_k} = \sum_{k=1}^{N} (\overline{Q}_{ij})_k t_k \Delta_k \overline{Z}_k \tag{19}$$

$$(B_{ij})_{\Delta_k} = \sum_{k=1}^{N} (\overline{Q}_{ij})_k (t_k \Delta_k \overline{Z}_k^{\,2} + (t_k\Delta_k)^3/12) \tag{20}$$

Engineering constants are then calculated from these new stiffness matrices, such as the effective stiffness E_Δ in Fig. 4 for the calculation of the failure strain. This will lead to a possibility of calculation of failure strain ε_{test}. Since a point-by-point modeling of non-linear elastic behavior up to failure is not the aim of this study, a bilinear model was used to describe the behavior beyond the virtual yield stress σ_Y. The results of modeling are compared with the experimental results in Section 4.3.

3.4. Manufacturing factor

Due to the variations in the manufacturing process of CMCs, the previously presented modeling approaches are upgraded by introducing a manufacturing factor Ω_k. The factor Ω_k takes FVC, porosity (e') and the angle between fiber orientation and occurring stress into account. The manufacturing process of the material results in variations in FVC and e' of the composite, which are decisive for the mechanical properties of the component. With the assumption that each UD-layer has identical fiber volume content and homogeneous porosity on a macroscopic scale, a linear mixing rule for the compound property can be modified to determine the manufacturing factor Ω_k of each equivalent UD-layer k. Using the normal linear model the compound property with the influence of property A and property B can be defined as:

$$\begin{aligned} &\textit{The compound property} = \textit{Property A}*\textit{Proportion of A} \\ &\qquad + \textit{Property B}*\ \textit{Proportion of B} \end{aligned}$$

The manufacturing factor Ω_k of WHIPOX™, is defined by the combination of influence of FVC, e' and angle of fiber orientation between the average values of the laminate and the actual values of layer k. *Property A* is the ratio of the actual FVC_k of the layer to the average $\overline{FVC}$ of the laminate. *Property B* takes ratio of the average $\bar{e}'$ to e'_k into consideration. With consideration of the mechanisms of influence of FVC on the fiber dominated direction and e' on matrix dominated direction: the *Proportion of A*, defined as the angle between the fiber orientation of the layer k and the occurring stress, is related to the FVC dominated direction; on the other hand, *Proportion of B* includes the angle between the fiber orientations of the layer k to the perpendicular direction of occurring stress and is considered to be the e' dominated direction. The value "$\theta_k/90$" serves as the proportion of the ratio of the porosity. As *Property A* and *B* together form a complete compound property with individual contributions, the sum of *Proportion of A* and *Proportion of B* is 100%. Therefore, the value "$1-(\theta_k/90)$" is assigned to the *Proportion of A*. With this information, the manufacturing factor Ω_k can be determined with the following equation:

$$\Omega_k = \left(\frac{FVC_k}{\overline{FVC}}\right)\left(1-\frac{\theta_k}{90}\right) + \left(\frac{\bar{e}'}{e'_k}\right)\left(\frac{\theta_k}{90}\right) \tag{21}$$

The manufacturing factor Ω_k is defined as a property of a layer in a particular laminate because it is calculated for individual layers factoring in the angle between the fiber orientation of the layer k and the occurring stress. With this definition, it is justifiable to use Ω_k when layer properties are assembled into the individual sub-matrices: strain stiffness $[S_{ij}]$, coupling stiffness $[C_{ij}]$ and bending stiffness $[B_{ij}]$. Therefore, Eqs. (18)–(20) from Section 3.3 are rewritten as Eqs. (22)–(24):

$$(S_{ij})_{\Delta_k,\Omega_k} = \sum_{k=1}^{N} (\overline{Q}_{ij})_k t_k \Delta_k \Omega_k \tag{22}$$

$$(C_{ij})_{\Delta_k,\Omega_k} = \sum_{k=1}^{N} (\overline{Q}_{ij})_k t_k \Delta_k \Omega_k \overline{Z}_k \tag{23}$$

$$(B_{ij})_{\Delta_k,\Omega_k} = \sum_{k=1}^{N} (\overline{Q}_{ij})_k (t_k \Delta_k \Omega_k \overline{Z}_k{}^2 + (t_k \Delta_k \Omega_k)^3/12) \tag{24}$$

It should be noted that the manufacturing factor Ω_k is not a characteristic value of the UD-layer but only quantifies the inhomogeneity in different laminates. This implies that the calculated properties of the equivalent UD-layer are independent of different plates for analytical modeling. The previous study of Shi et al. [24] has shown that a modified stiffness matrix with consideration of factor Ω_k leads to a precise prediction of the elastic properties of wound CMCs. The effect of factor Ω_k over the modeling results for the tensile failure properties is discussed in the following sections.

4. Results and discussion

4.1. Experimental results

The typical tensile stress-strain behaviors of WHIPOX™-NC and -WC with different fiber orientations are summarized in Fig. 5. The longitudinal and transverse strains are presented. The indications, for example ± 3°, denote the angles between fiber and loading directions (see Table 2). The stress-strain response of WHIPOX™ strongly depends on the loading direction. With ± 3° and ± 15° orientations, the composites show an almost linear behavior with higher stiffness and strength as seen in Fig. 5a. Since the fibers are oriented close to the loading direction, the matrix is able to transfer the applied load to the fibers. In contrast, under ± 67.5° and ± 75° tensile loading the composite shows an almost linear behavior as well but stiffness and the strength values are considerably lower (in Fig. 5b). This is mainly due to the dominating weak matrix in this loading direction. Scanning electron microscopy (SEM) pictures of the tensile fracture surface explain the dependence between tensile properties and fiber orientation: considerable fiber pull-out effect can be observed in Fig. 6a for fiber orientation ± 15° with higher stiffness and strength; Fig. 6b showed clearly that the samples in ± 75° is matrix dominated direction and had much lower mechanical properties. Furthermore, WHIPOX™ with matrix cracks (see Section 2.1) under ± 30°, ± 45° and ± 60° tensile loading shows nonlinear behavior (Fig. 5a). This can be assumed that the damage in matrix and the effects of energy dissipation of matrix cracks lead to a significant degradation of the composite's properties in this loading direction. The fracture surface of coupon with fiber orientation ± 45° was analyzed through SEM and some fiber pull-out effect can be

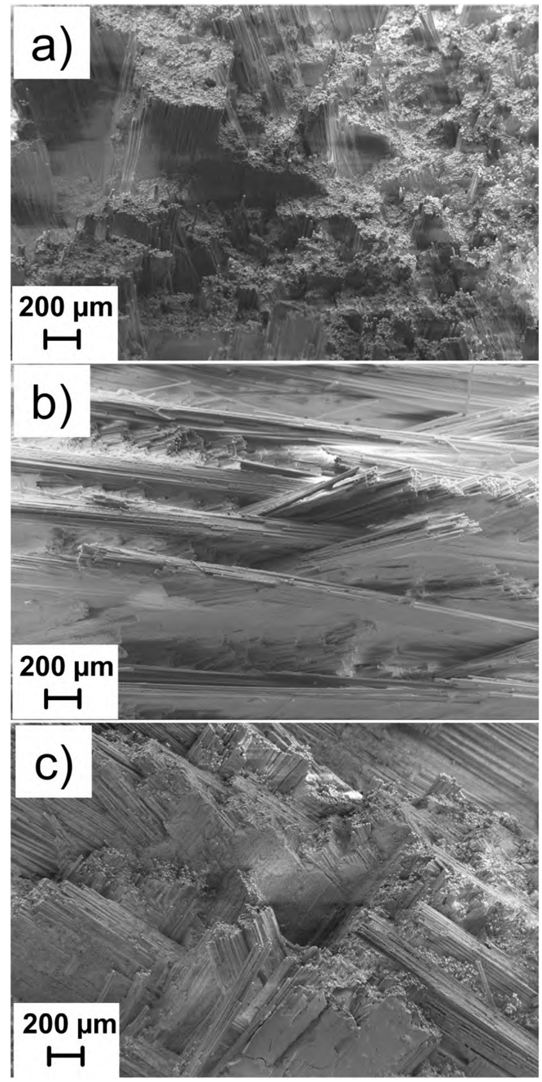

Fig. 6. SEM images for the tensile fracture surface of samples with different fiber orientations: (a) fiber orientation ± 15°; (b) fiber orientation ± 75°; (c) fiber orientation ± 45°.

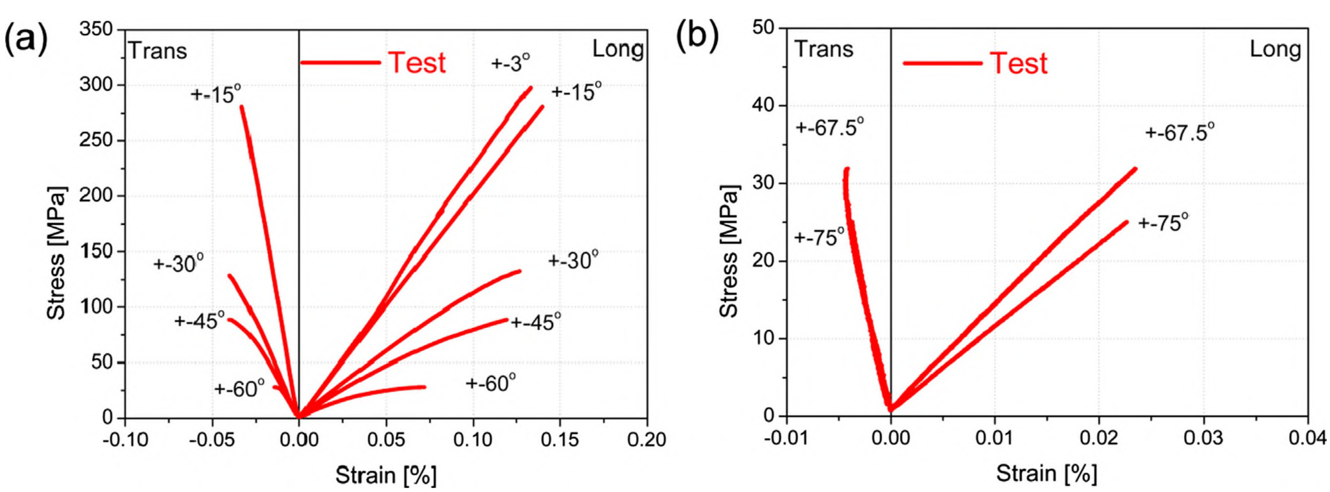

Fig. 5. Stress-strain behaviors of WHIPOX™ with different fiber orientations under tensile load. (For interpretation of the references to colour in this figure legend, the reader is referred to the web version of this article.)

observed in Fig. 6c, which indicate that the mechanical properties of orientation ± 45° under tensile loading is higher than the coupon with orientation ± 75° but lower than the coupon with ± 15° (Table 3). The comparison of test and modeling results of stress-strain behaviors are shown and discussed in Section 4.3.

The tensile strength σ of different winding angles were calculated from the maximum force according to DIN EN 658-1 [44]. The fracture strain value ε of the tensile test was defined as the strain value at maximum tensile strength. The determined strengths σ and ultimate strain ε are listed in Table 3. The indices x and y correspond to the indications from Fig. 1b. For orthogonal orientations of ± 45°, the strength values σ_x and σ_y are same and the ultimate strain ε_x is equal to ε_y. *FVC* and open porosity e' scatter in a wide range and the individual value of different plates are shown in Table 3. The influence of different *FVC* and e' on the material properties with the help of the manufacturing factor Ω_k is discussed in the following sections.

4.2. Modeling of failure stresses

Due to the lack of representative experimental data of the actual UD-layer for CMCs, the strength values of equivalent UD-layer were fitted to different test results from the investigated material WHIPOX™. It should be noticed that the test results under compression and shear load have been summarized in previous study [33] and are not discussed in this work. The approximated strength properties with the inclusion of different micro-structures, UD-WC (UD-layer with cracks) and UD-NC (UD-layer no cracks) (see Section 2.1), are enumerated in Table 4. UD-WC corresponds to winding angles of ± 30° to ± 45° and UD-NC applies to angles smaller than ± 30° and bigger than ± 60°. The indices 1 and 2 correspond to the indications in Fig. 3 where 1 is in the fiber direction and 2 is transverse to the fiber direction.

Based on the approximated strength properties in Table 4, a 3D visualization with help of MATLAB R2013a for WHIPOX™ depicting matrix cracks (red envelope) and without matrix cracks (grey envelop) is shown in Fig. 7. It outlines the failure regions of these two different groups.

By using the strength ratio R of the Tsai-Wu failure criterion, the tensile strength of the laminate with a symmetric fiber orientation can be predicted. Fig. 8 shows the test results (from Table 3) with different fiber orientations and calculated failure strengths for the material WHIPOX™. This is depicted with (UD-WC) and without the matrix cracks (UD-NC) under tensile load. The modeling curve in Fig. 8 is the result calculated without consideration of the manufacturing factor Ω_k for different plates. A distinct inconsistency at ± 60° can be observed in the curve due to the changes in microstructure.

Although a relatively good correlation between the modeling results and some experiments can be observed in Fig. 8, in order to upgrade the analytical approach with consideration of fiber volume content and open porosity in different plates, the manufacturing factor Ω_k value is coupled with individual sub-matrices for the modeling of failure strength. By using Eq. (21) presented in Section 3.4 the manufacturing factor Ω_k was calculated for the plates listed in Table 3. Because the fiber orientation was symmetrical to the test direction for all tested samples, Ω_k for each individual layer is identical for the same fiber orientation of whole laminate and summarized in Table 5. The results show a maximum Ω_k equal to 1.35 for plate BT225 in the ± 67.5° direction, which has relatively low porosity (18.5%). They also show a minimum value of 0.86 for plate BT30 in ± 30° direction due to the low

Table 4
The estimated strength values of the equivalent UD-layer of WHIPOX™.

Strength	σ_1^T [MPa]	σ_2^T [MPa]	σ_1^C [MPa]	σ_2^C [MPa]	τ_{12} [MPa]
UD-WC	279.0	22.5	− 243.0	− 45.0	65.0
UD-NC	279.0	22.0	− 274.0	− 120.0	85.0

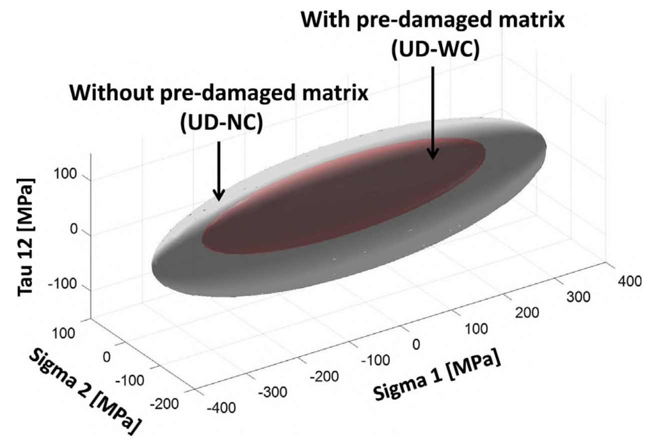

Fig. 7. 3D representation of Tsai-Wu failure criterion in stress space for material WHIPOX™. (For interpretation of the references to colour in this figure legend, the reader is referred to the web version of this article.)

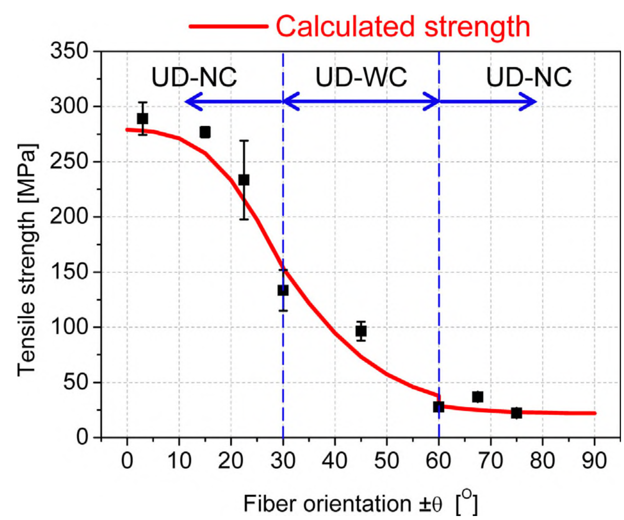

Fig. 8. Original experimental data with different fiber orientation (black symbols) and predicted failure strength (curves) for WHIPOX™ depicting with (UD-WC) and without matrix cracks (UD-NC) under tensile load. (For interpretation of the references to colour in this figure legend, the reader is referred to the web version of this article.)

fiber volume content (34.0%). The results of the manufacturing factor Ω_k in Table 5 show that: due to the variations in the manufacturing process of WHIPOX™ the *FVC* and open porosity scatter in a wide range by different batches; the factor Ω_k with consideration of different fiber volume contents, porosities and the angles between fiber orientation and occurring stress should be used to qualify uncertainties in the laminate during the manufacturing process. The effect of Ω_k for the modeling results are shown in Fig. 9 and a more precise prediction of failure strength can be observed.

4.3. Modeling of failure strain

The tensile stress-strain curves of WHIPOX™ with fiber orientations of ± 30°, ± 45° and ± 60° in Fig. 5a show inelastic behavior up to failure. In this case, the failure strength and strain cannot be directly correlated with the Tsai-Wu failure criterion in stress and strain spaces. The inelastic deformation factor Δ_k presented in Section 3.3 is defined as the relationship between calculated linear strain value ε_{linear} and real failure strain ε_{test}: $\Delta_k = \varepsilon_{linear}/\varepsilon_{test}$ (see Eq. (13)). If $\Delta_k = 1$, then linear elastic behavior up to failure is shown. The calculated values (black symbols) of the inelastic deformation factor Δ_k from the investigated

Table 5
Summary of the calculated manufacturing factor Ω_k and inelastic deformation factor Δ_k of different plates and fiber orientations.

Plate	WF3	BT15		BT225		BT30		BT45
Fiber orientation	± 3°	± 15°	± 75°	± 22.5°	± 67.5°	± 30°	± 60°	± 45°
Ω_k	1.09	1.04	0.98	1.11	1.35	0.86	0.87	0.98
Δ_k	1	1	1	1	1	0.802	0.604	0.703

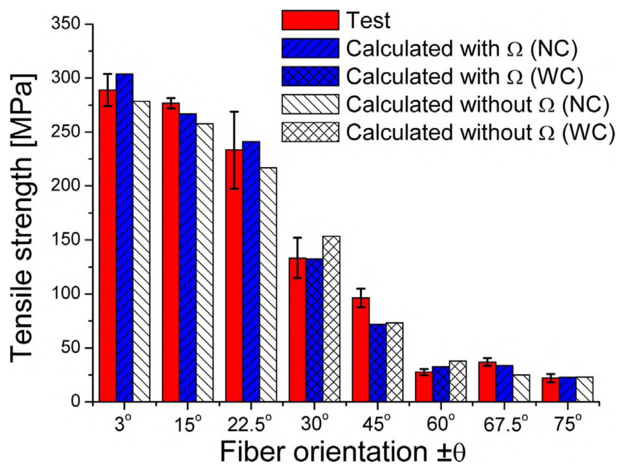

Fig. 9. Comparison of calculated failure strength with and without consideration of manufacturing factor $\mathbf{\Omega_k}$ to test results of wound WHIPOX™ under tensile load. (For interpretation of the references to colour in this figure legend, the reader is referred to the web version of this article.)

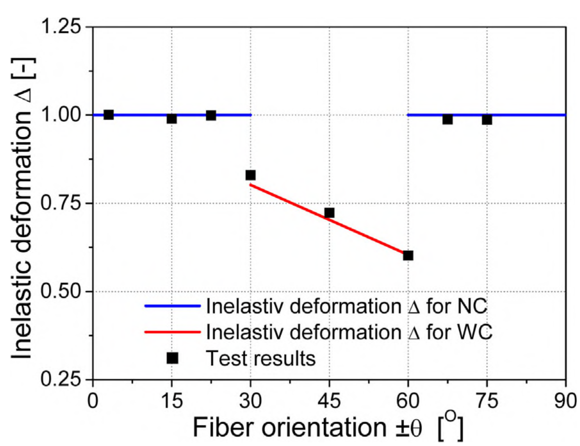

Fig. 10. Calculated inelastic deformation factor $\mathbf{\Delta_k}$ (black symbols) from the investigated material WHIPOX™ with different fiber orientations. (For interpretation of the references to colour in this figure legend, the reader is referred to the web version of this article.)

material WHIPOX™ with different fiber orientations are shown in Fig. 10. It can be observed that the laminates in the area without matrix cracks (NC) exhibit linear stress-strain behavior with Δ equal to approx. 1.0. In comparison, the value of Δ_k is strongly dependent on the fiber orientation of the laminate in the area with matrix cracks (WC). A function can be established by fitting the calculated results Δ between ± 30° and ± 60° in Fig. 10. The inelastic deformation factor Δ_k depicting the areas without matrix cracks (NC) and with matrix cracks (WC) is defined as:

$$\begin{aligned} WHIPOX{-}NC&: \Delta_k = 1.0 \\ WHIPOX{-}WC&: \Delta_k = (-6.6E{-}3)\theta + 1.0 \end{aligned} \tag{25}$$

where θ is the angle between fiber orientation and the loading direction.

The different behavior can be explained by the micro structure in the WC area with matrix cracks. The non-linear behavior is most probably induced by cracks in the matrix under a certain load. The already existing shrinkage cracks in the WHIPOX™-WC matrix show strong dependence on the angle between fiber orientation and the occurring loading. For WHIPOX™ without matrix cracks, a linear behavior with Δ_k equal to 1 is expected. In the case of tensile loading in fiber direction of a virtual UD-layer with cracks, the fiber properties are dominated in this direction and the matrix and shrinkage cracks have limited influence. Therefore, the material behavior is assumed as linear elastic up to failure with the value of factor Δ_k equals to 1.0. This agrees with the calculated results from second part of Eq. (25) with $\theta = 0$. On the other hand, in case of loading in transverse fiber direction, the matrix dominates the mechanical behavior and a significant non-linear behavior with low Δ_k value can be expected. It is important to note that the evaluation of factor Δ_k uses both approximation and physically-based methods in order to characterize WHIPOX™ inelastic behavior. The inelastic deformation factor Δ_k is defined as a mathematical equation that is incorporated into the material modeling relation and solved by using the analysis of microstructure of the investigated material WHIPOX™.

To explain the performance of modeling approach with inelastic deformation factor Δ_k for failure strain and stress-strain behavior, the Δ_k value of tensile samples with fiber orientation of ± 15° and ± 30° have been first calculated as examples. Based on the microstructure analysis of matrix cracks [23,24], no shrinkage cracks are visible for ± 15° (WHIPOX-NC). Therefore, according to the first part of Eq. (25) the value of factor Δ_k for ± 15° orientation equals to 1.0. In comparison, the value of Δ_k for the sample with orientation of ± 30° is approx. 0.802, which is calculated from the second part of Eq. (25) for the material WHIPOX-WC. As presented in Section 3.3, the factor Δ_k is assembled into the individual sub-matrices: strain stiffness $[S_{ij}]$, coupling stiffness$[C_{ij}]$ and bending stiffness $[B_{ij}]$, for the calculation of the engineering constants of a virtual equivalent UD-layer of WHIPOX™. In this way, the failure strain can be estimated. For WHIPOX™-NC with Δ_k equals to 1.0, e.g. ± 15°, the initial stiffness matrix remains unchanged up to the failure and the calculated failure strain is approx. 0.134. On the other hand, a bilinear model was used to describe the behavior of WHIPOX™-WC beyond the virtual yield stress σ_Y calculated in Eq. (14). For example, for the fiber orientation ± 30°: the modulus E_Δ with non-linear behavior (Fig. 4) is approx. 102.7 GPa, which is calculated through the sub-matrices with consideration of deformation factor Δ_k; and the calculated failure strain is approx. 0.129 for the ± 30° orientation. The inelastic deformation factor Δ_k is dependent on the fiber orientation and the microstructure (WC or NC). The value of Δ_k for each layer is summarized in Table 5.

The comparison of longitudinal and transverse stress-strain behavior of WHIPOX™-NC and WHIPOX™-WC as seen in test and calculated results are summarized in Fig. 11. The behavior of fiber orientations ± 3° and ± 15° (in Fig. 11a) and ± 67.5° and ± 75° (in Fig. 11b) are linear in the laminate of WHIPOX™-NC. The non-linear behavior up to failure of the laminate of WHIPOX™-WC with the fiber orientations ± 30°, ± 45° and ± 60° are compared with the bilinear model results in Fig. 11a. A bar diagram for the comparison of calculated failure strain depicting WHIPOX™-NC and -WC with the tensile test results for wound WHIPOX™ with different fiber orientations is shown

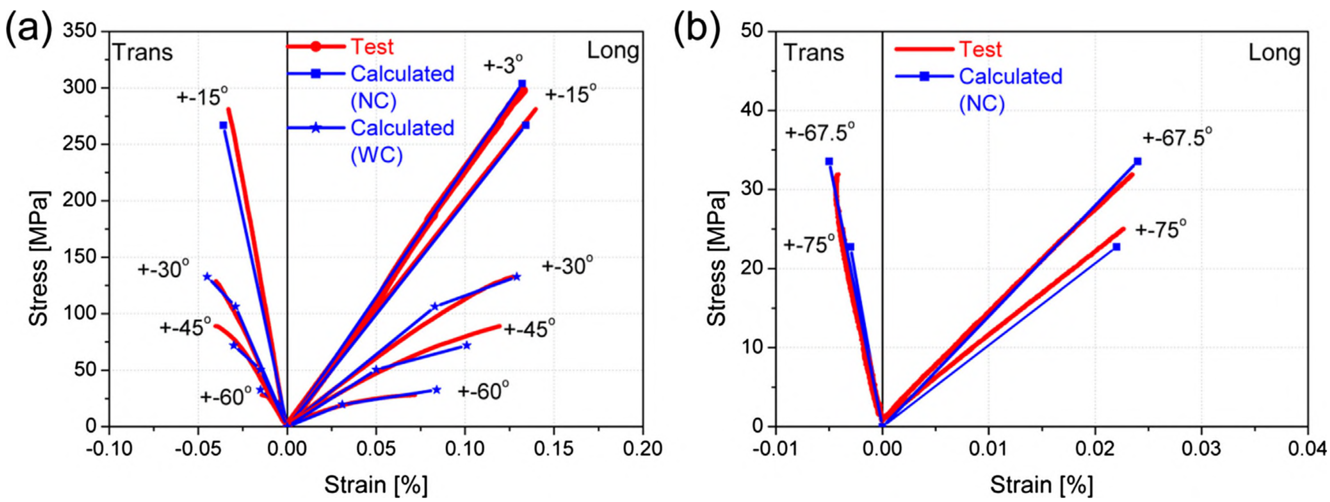

Fig. 11. Tensile stress-strain comparison diagrams with test results and calculated results for laminate WHIPOX™-NC and WHIPOX™-WC with fiber orientations (a) from ± 3° to ± 60° and (b) ± 67.5° and ± 75°. (For interpretation of the references to colour in this figure legend, the reader is referred to the web version of this article.)

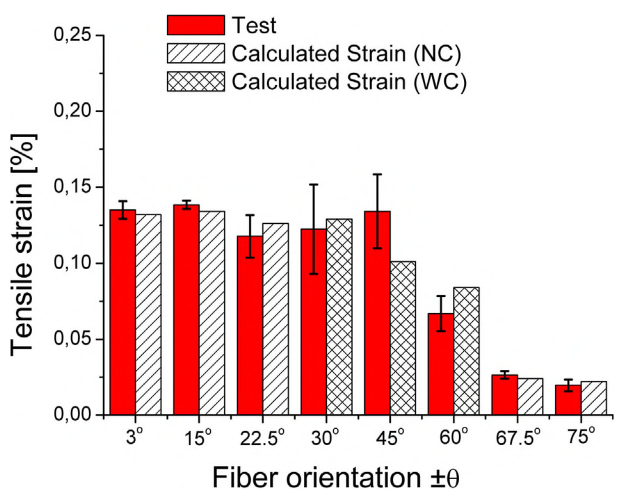

Fig. 12. Comparison of calculated failure strains of WHIPOX™-NC and WHIPOX™-WC with tensile test results for WHIPOX™ with different fiber orientations. (For interpretation of the references to colour in this figure legend, the reader is referred to the web version of this article.)

in Fig. 12. A very close correlation can be observed in Figs. 11 and 12 for the measured and predicted failure strain. Due to the fact that the Ω_k value is coupled with the layer thickness t_k for the calculation of the stiffness matrices $(S_{ij})_{\Delta_k,\Omega_k}$, $(C_{ij})_{\Delta_k,\Omega_k}$ and $(B_{ij})_{\Delta_k,\Omega_k}$ in Section 3.4, the influence of different FVC, e' and angle of fiber orientation from different plates has been taken into consideration in the modeling of elastic properties (see previous studies of Shi et al. [24]) and strength (Section 4.2). Therefore, for the modeling of the strain value, the influence of Ω_k can be hypothesized to $(\Omega_k)(\Omega_k)^{-1}$. As a result, the impact of Ω_k on the strain is negligible.

4.4. Application of modeling approaches to wound C/C-SiC material

The modeling approaches developed and presented in this study can be applied to predict the mechanical properties of other CMCs, e.g. wound C/C-SiC developed by Institute of Structures and Design, German Aerospace Center Stuttgart. Based on the tensile strengths in the works of Breede [45,46], the approximated strength values of the equivalent UD-layer are enumerated in Table 6. Due to the lack of values concerning results of compressive testing in [45,46], the strength parameters F_1 to F_{66} of Tsai-Wu failure criterion in stress space are calculated using only the tensile strength of the equivalent UD-layer in Table 6 ($\sigma_1^T = \sigma_1^C$ and $\sigma_2^T = \sigma_2^C$). The shear strength (τ_{12}) is taken from an existing report [47]. Similar to material WHIPOX™, the interaction term F_{12} from the Tsai-Wu equation has been set to zero.

Table 6
Summary of the estimated strength values and the inelastic deformation factorΔ_k for wound C/C-SiC material parameter sets.

Strength values	$\sigma_1^T = \sigma_1^C$ [MPa]	$\sigma_2^T = \sigma_2^C$ [MPa]	τ_{12} [MPa]
	230.0	35.0	80.0
Δ_k	$\Delta_k = (-0.015)\theta + 1.225$: Orientation ± 30° to ± 60° $\Delta_k = 1$: Orientation 0° to ± 15° & ± 75° to 90°		

By using the strength ratio R of the Tsai-Wu failure criterion, which has been presented for material WHIPOX™, the tensile strengths of the wound C/C-SiC with different fiber orientations can be predicted. Fig. 13a shows the original test results (from [45,46]) with different fiber orientations and calculated failure strengths. The stress-strain response of wound C/C-SiC strongly depends on the loading direction. The composites under ± 30°, ± 45° and ± 60° under tensile loading show non-linear elastic behavior and with ± 15° and ± 75° orientations the composites show an almost linear behavior in [45,46]. Therefore, similar to material WHIPOX™, an inelastic deformation factor Δ_k was evaluated for the fiber orientations between ± 30° and ± 60° (Table 6). A bar diagram for the comparison of calculated failure strain with the tensile test results for wound C/C-SiC with different fiber orientations is shown in Fig. 13b. A variety of different fiber orientations lead to different mechanical behaviors of wound C/C-SiC. This can be explained by the presence of different microstructure, which consequently influences the resulting material properties. On the one hand, similar microstructure of fiber orientations ± 30° (± 60°) and ± 45° can be observed in [45,46]. On the other hand, due to the reduced hindrance of shrinkage during the manufacturing process, the matrix width of winding angle ± 15° (± 75°) is clearly narrower (see [45,46]). Therefore, an identical definition of Δ cannot be applied for the fiber orientation between ± 0° to ± 30° and ± 60° to ± 90°. According to the stress-strain curves in [45,46], almost linear elastic behavior can be obtained for material C/C-SiC with winding angle 15° and 75°. Therefore, the failure strains of fiber orientation between ± 0° to ± 30° and ± 60° to ± 90° were calculated with $\Delta_k = 1$ (Table 6) and shown in Fig. 13b. This phenomenon is comparable to the modeling approaches for material WHIPOX™ with two different groups WC with inelastic deformation and NC without inelastic deformation. A strong correlation

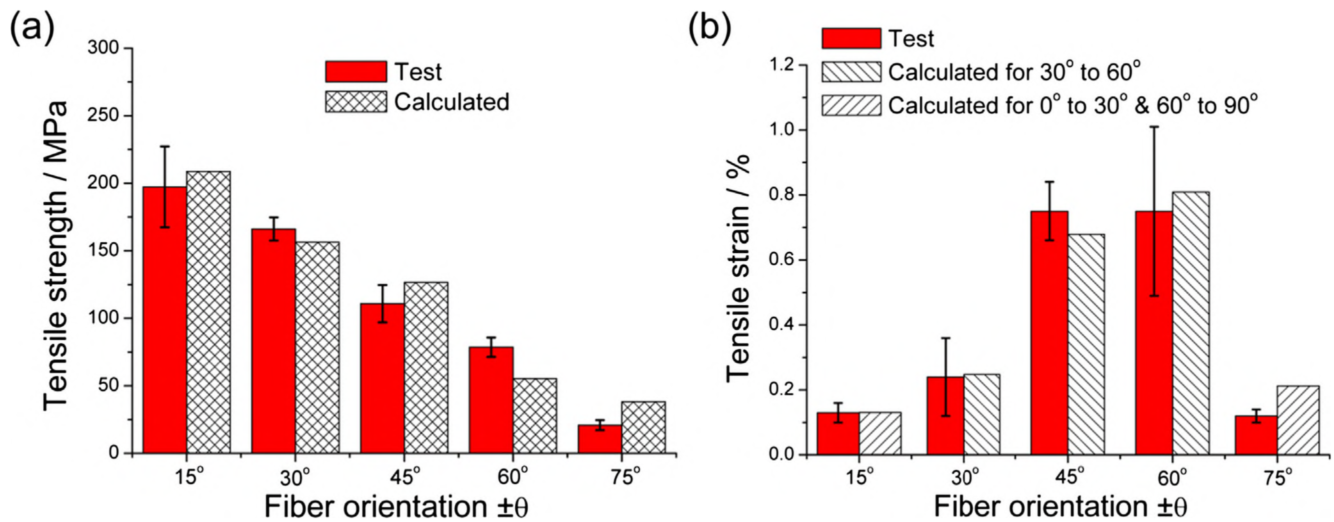

Fig. 13. Comparison of calculated results to original experimental data of wound C/C-SiC, (a) tensile strength and (b) tensile strain. (For interpretation of the references to colour in this figure legend, the reader is referred to the web version of this article.)

can be observed in Fig. 13a and b for the measured and predicted failure values.

5. Conclusions

The present work has demonstrated that the mechanical behavior of wound ceramic composites with various fiber orientations may be described using macroscopic constitutive modeling approaches. Compared to the previous studies of prediction of elastic properties in [23,24], this work focused on the investigation and modeling of tensile failure properties for wound CMCs through modified Tsai-Wu failure criterion.

First, all modeling approaches developed in this study are dependent on experimental determination and microstructure analysis. The material's characteristic values under tensile loading of the investigated material WHIPOX™ in different wound orientations were evaluated with in-plane tension test. Based on the microstructure analysis of shrinkage cracks of WHIPOX™ through Micro Computed Tomography, the modeling of the properties of WHIPOX™ was divided into two classes: WHIPOX™ with matrix cracks (WC) and WHIPOX™ without matrix cracks (NC).

Then, due to the lack of the required matrix and fiber properties within the manufactured composite and due to the unavailable representative characteristics of CMC UD-materials, it was demonstrated that classic failure criterion cannot be directly adapted to describe the material behavior of wound CMCs. Therefore, advanced modeling approaches with virtually equivalent UD-layer properties are created for the evaluation and prediction of the material properties under tensile loading for wound CMC materials. The strength properties were calculated and evaluated by fitting different test results to modified Tsai-Wu criterion and failure strain by using the inelastic deformation behavior factor Δ_k. All the values are discussed and calculated with consideration given to different microstructures with or without matrix cracks.

Furthermore, the modeling approaches developed in this study may be applied to different fiber reinforced composites manufactured by the winding process with consideration of particular features of investigated material. For the investigated composite WHIPOX™, some material specialties are implemented in the modeling approaches:

- Division of material modeling groups into two classes (WHIPOX™-WC and –NC) based on the microstructural analysis.
- Interaction between failure strength and strain through inelastic deformation factor Δ_k.
- Update of the analytical model through manufacturing factor Ω_k for different plates with different fiber volume contents and porosities.

Finally, modeling approaches for the prediction of the material properties of wound ceramic composites were presented. The most important results of this study are:

- Tensile strength values of the laminate with different fiber orientations can be predicted using the strength ratio R of the Tsai-Wu failure criterion.
- A modified stiffness matrix with the inelastic deformation factor Δ_k and manufacturing factor Ω_k leads to a precise calculation of failure properties and has been used to describe the inelastic stress-strain behavior.

Based on the good correlation between the experiments and the modeling results, it can be shown that modeling approaches factoring in the above mentioned particular material features allow for a very accurate prediction of the mechanical properties for CMC laminates under in-plane tensile loading. The present work has identified a general modus operandi going from experimental determination and microstructure analysis to the prediction of the mechanical behavior of wound CMCs with varied fiber orientations. The results of this work are of great value for the future design and development of this class of composites. In this way the application of CMC-components in new fields like aerospace and civil engineering may be enhanced.

Acknowledgment

We want to thank Dr. Stefan Hackemann, DLR, Institute of Materials Research and Dr. Severin Hofmann, DLR, Institute of Structures and Design, for the collaboration and support for this work.

References

[1] Christin F. CMC materials for space and aeronautical applications. Ceramic matrix composites. Wiley-VCH Verlag GmbH & Co. KGaA; 2008. p. 327–51.
[2] Kohyama A. CMC for nuclear applications. Ceramic matrix composites. Wiley-VCH Verlag GmbH & Co. KGaA; 2008. p. 353–84.
[3] Gerendás M, Cadoret Y, Wilhelmi C, Machry T, Knoche R, Behrendt T, et al. Improvement of Oxide/Oxide CMC and development of combustor and turbine components in the HiPOC program. In: ASME 2011 Turbo Expo: Turbine Technical Conference and Exposition; 2011. p. 477–90.
[4] Behrendt T, Hackemann S, Mechnich P, Shi Y, Hönig S, Hofmann S, et al. Development and test of oxide/oxide cmc combustor liner demonstrators for aero engines. In: ASME 2016 Turbo Expo: turbine technical conference and exposition;

2016.
[5] Herbell TP, Eckel AJ. Ceramic matrix composites for rocket engine turbine applications. J Eng Gas Turb Power 1993;115(1):64–9.
[6] Schmidt S, Beyer S, Knabe H, Immich H, Meistring R, Gessler A. Advanced ceramic matrix composite materials for current and future propulsion technology applications. Acta Astronaut 2004;55(3–9):409–20.
[7] Low I-M. Ceramic matrix composites: microstructure, properties and applications. Cambridge, England: Woodhead Pub. and Maney Pub. on behalf of the Institute of Materials, Minerals & Mining; 2006.
[8] Göring J, Hackemann S, Kanka B. WHIPOX (R): a fiber-reinforced oxide-ceramic matrix composite for long-term high-temperature applications. Materialwiss Werkstofftech 2007;38(9):766–72.
[9] Breede F, Jemmali R, Voggenreiter H, Koch D. Design and testing of a C/C-SiC nozzle extension manufactured via filament winding technique and liquid silicon infiltration. Design, development, and applications of structural ceramics, composites, and nanomaterials. John Wiley & Sons, Inc; 2014. p. 1–14.
[10] Zhao W, Liaw PK, Yu NI. Computation of the lamina stacking sequence effect on elastic moduli of a plain-weave Nicalon/SiC laminated composite with a [0/30/60] lay-up. J Nucl Mater 1998;253(1–3):10–9.
[11] Carey J, Munro M, Fahim A. Longitudinal elastic modulus prediction of a 2-D braided fiber composite. J Reinf Plast Compos 2003;22(9):813–31.
[12] Srikanth L, Rao RMVGK. Concurrent studies on braided and filament wound carbon fiber composites - a comparative appraisal. J Reinf Plast Comp 2011;30(16):1359–65.
[13] Xu L, Kim SJ, Ong CH, Ha SK. Prediction of material properties of biaxial and triaxial braided textile composites. J Compos Mater 2012;46(18):2255–70.
[14] Tsai SW, Wu EM. A general theory of strength for anisotropic materials. J Compos Mater 1971;5(1):58–80.
[15] Puck A, Schürmann H. Failure analysis of FRP laminates by means of physically based phenomenological models. Compos Sci Technol 2002;62(12–13):1633–62.
[16] Tushtev K, Horvath J, Koch D, Grathwohl G. Deformation and failure modeling of fiber reinforced ceramics with porous matrix. Adv Eng Mater 2004;6(8):664–9.
[17] Lamon J. Approach to microstructure–behavior relationships for ceramic matrix composites reinforced by continuous fibers. In: Bansal NP, Lamon J, editors. Ceramic matrix composites. John Wiley & Sons, Inc.; 2014. p. 520–47.
[18] Chawla N. Effect of laminate stacking sequence on the high frequency fatigue behavior of SCS-6 fiber-reinforced Si3N4 matrix composites. Metall Mater Trans A 1997;28(11):2423–7.
[19] Chawla N, Tur YK, Holmes JW, Barber JR, Szweda A. High-frequency fatigue behavior of woven-fiber-fabric-reinforced polymer-derived ceramic-matrix composites. J Am Ceram Soc 2005;81(5):1221–30.
[20] Chawla N, Liaw PK, Lara-Curzio E, Ferber MK, Lowden RA. Effect of fiber fabric orientation on the flexural monotonic and fatigue behavior of 2D woven ceramic matrix composites. Mater Sci Eng A 2012;557:77–83.
[21] Van Paepegem W, Degrieck J. Calculation of damage-dependent directional failure indices from the Tsai–Wu static failure criterion. Compos Sci Technol 2003;63(2):305–10.
[22] Sevenois RDB, Van Paepegem W. Fatigue damage modeling techniques for textile composites: review and comparison with unidirectional composite modeling techniques. Appl Mech Rev 2015;67(2):021401.
[23] Shi Y, Hofmann S, Jemmali R, Hackemann S, Koch D. Determination of elastic properties for a wound oxide ceramic composite. J Ceramic Sci Technol 2013;5(1):31–8.
[24] Shi Y, Jain N, Jemmali R, Hofmann S, Koch D, Hackemann S. Prediction of elastic properties for a wound oxide ceramic matrix composite material. Int J Appl Ceram Technol 2015;12:E99–110.
[25] Cuntze RG, Freund A. The predictive capability of failure mode concept-based strength criteria for multidirectional laminates. Compos Sci Technol 2004;64(3–4):343–77.
[26] Puck A, Kopp J, Knops M. Guidelines for the determination of the parameters in Puck's action plane strength criterion. Compos Sci Technol 2002;62(3):371–8.
[27] Hinton MJ, Kaddour AS, Soden PD. Failure criteria in fibre reinforced polymer composites: the World-Wide Failure Exercise. Oxford, UK: Elsevier Science Ltd.; 2004.
[28] Hinton MJ, Kaddour AS. The background to the second world-wide failure exercise. J Compos Mater 2012;46(19–20):2283–94.
[29] Kaddour AS, Hinton MJ, Smith PA, Li S. The background to the third world-wide failure exercise. J Compos Mater 2013;47(20–21):2417–26.
[30] Rohwer K. Predicting fiber composite damage and failure. J Compos Mater 2015;49(21):2673–83.
[31] Schmücker M, Mechnich P. All-oxide ceramic matrix composites with porous matrices. In: Krenkel W, editor. Ceramic matrix composites. Wiley-VCH Verlag GmbH & Co. KGaA; 2008. p. 205–29.
[32] Schmücker M, Grafmüller A, Schneider H. Mesostructure of WHIPOX all oxide CMCs. Compos A Appl Sci Manuf 2003;34(7):613–22.
[33] Shi Y. Characterization and modeling of the mechanical properties of wound oxide ceramic composites. Karlsruhe, Germany: Karlsruher Institut für Technologie (KIT); 2017.
[34] Jones RM. Mechanics of composite materials. second ed. Taylor & Francis Inc.; 1998.
[35] Liu KS, Tsai SW. A progressive quadratic failure criterion for a laminate. Compos Sci Technol 1998;58(7):1023–32.
[36] Kuraishi A, Tsai SW, Liu KKS. A progressive quadratic failure criterion, part B. Compos Sci Technol 2002;62(12–13):1683–95.
[37] Tsai SW, Melo JDD. Composite Materials Design and Testing: Composites Design Group; 2015.
[38] Wu EM. Optimal experimental measurements of anisotropic failure tensors. J Compos Mater 1972;6(4):472–89.
[39] Narayanaswami R, Adelman HM. Evaluation of the tensor polynomial and hoffman strength theories for composite materials. J Compos Mater 1977;11(4):366–77.
[40] Lin W-P, Hu H-T. Parametric study on the failure of fiber-reinforced composite laminates under biaxial tensile load. J Compos Mater 2002;38(12):1481–503.
[41] Ellul B, Camilleri D, Betts JC. A progressive failure analysis applied to fiber-reinforced composite plates subject to out-of-plane bending. Mech Compos Mater 2014;49(6):605–20.
[42] Tsai SW. Composites design - 1985 United States air force materials laboratory. USA: Think Composites; 1985.
[43] Kaw AK. Mechanics of composite materials. second ed. CRC Press; 2005.
[44] DIN EN 658-1: Advanced technical ceramics - Mechanical properties of ceramic composites at room temperature - Part 1: Determination of tensile properties; 1999.
[45] Breede F. Entwicklung neuartiger faserkeramischer C/C-SiC verbundwerkstoffe auf basis der wickeltechnik für raketendüsen. Stuttgart, Germany: University Stuttgart; 2017.
[46] Breede F, Koch D, Maillet E, Morscher GN. Modal acoustic emission of damage accumulation in C/C–SiC composites with different fiber architectures. Ceram Int 2015;41(9):12087–98.
[47] Geinitz S. Ermittlung des Schubmoduls von Faserverstärkter Keramik: Institut für Flugzeugbau der Universität Stuttgart und Institut für Bauweisen- und Konstruktionsforschung des DLR; 2006.
[48] Hackemann S, Behrendt T, Aumeier T, Richter T, Shi Y, Hofmann S, et al. Development and testing of a low NOx oxide ceramic combustor for aero-engines. In: 39th international conference and expo on advanced ceramics and composites, Daytona Beach, USA; 2015.